PHYSICAL REVIEW B **90**, 100406(R) (2014)

Quantum dimer model for the spin-$\frac{1}{2}$ kagome Z_2 spin liquid

Ioannis Rousochatzakis,[1,2] Yuan Wan,[3] Oleg Tchernyshyov,[3] and Frédéric Mila[4]
[1]*Institute for Theoretical Solid State Physics, IFW Dresden, D-01069 Dresden, Germany*
[2]*Max Planck Institut für Physik Komplexer Systeme, Nöthnitzer Straße 38, 01187 Dresden, Germany*
[3]*Department of Physics and Astronomy, The Johns Hopkins University, Baltimore, Maryland 21218, USA*
[4]*Institute of Theoretical Physics, École Polytechnique Fédérale de Lausanne (EPFL), CH-1015 Lausanne, Switzerland*
(Received 3 August 2013; published 15 September 2014)

We revisit the description of the low-energy singlet sector of the spin-$\frac{1}{2}$ Heisenberg antiferromagnet on kagome in terms of an effective quantum dimer model. With the help of exact diagonalizations of appropriate finite-size clusters, we show that the embedding of a given process in its kagome environment leads to dramatic modifications of the amplitudes of the elementary loop processes, an effect not accessible to the standard approach based on the truncation of the Hamiltonian to the nearest-neighbor valence-bond basis. The resulting parameters are consistent with a Z_2 spin liquid rather than with a valence-bond crystal, in agreement with the last density matrix renormalization group results.

DOI: 10.1103/PhysRevB.90.100406 PACS number(s): 75.10.Jm, 75.10.Kt, 71.27.+a

Introduction. The spin $S = \frac{1}{2}$ kagome antiferromagnet (AFM) described by the Heisenberg model,

$$\mathcal{H} = J \sum_{\langle ij \rangle} \mathbf{S}_i \cdot \mathbf{S}_j \tag{1}$$

(where $\langle ij \rangle$ are nearest-neighbor sites and $J = 1$ in the following), has been established as one of the main candidates for realizing the long-sought quantum spin liquid [1–5], which has topological properties and fractionalized excitations (spinons) [6–9]. The recent discovery [10] of the herbertsmithite $ZnCu_3(OH)_6Cl_2$ has motivated a new burst of experimental and theoretical activity, as this layered compound is a nearly perfect realization of (1) and shows signatures of spin-liquid behavior [11].

On the theory front, there are several proposals for the nature of the ground state (GS), ranging from gapless critical phases [12–15], to gapped resonating valence bond crystals (VBC) [16–24], chiral [25,26], or topological spin liquids [27,28]. In principle, such magnetically disordered phases can be described by short-range valence bonds [1–4,29], and in fact there are good reasons to believe that the qualitative physics is captured by the nearest-neighbor valence bond (NNVB) basis. This effort goes back to Zeng and Elser [30], who showed that the NNVB dynamics is governed by several tunneling processes, cast in a quantum dimer model (QDM) form [8,22,23,31,32]. Whether this description leads to a valence-bond crystal or to a disordered phase is still open, however. Indeed, recent investigations of the unconstrained QDM by Poilblanc *et al.* [22,23] and by Läuchli [33] have shown that the GS is extremely sensitive to the competition between the elementary loop processes, and the answer relies on the precise determination of the corresponding QDM parameters.

Here, we develop a numerical approach to determine the effective QDM parameters. This approach is based on exact diagonalizations (ED) of appropriately chosen finite clusters, and thus captures the effect of longer-range singlets that are virtually excited around triangles without a valence bond, or "defect triangles" (see Fig. 1). This method thereby captures the dependence of the QDM amplitudes on the environment (i.e., the particular VB configuration away from the central hexagon involved in the elementary loop process), by contrast to the standard approach based on the truncation of the Hamiltonian to the NNVB basis, which is shown to lead to the same parameters regardless of the environment. This effect turns out to have dramatic consequences: the QDM parameters derived in this way are consistent with a Z_2 spin liquid rather than a valence-bond crystal.

Let us start by some general remarks about the QDM description of the low-energy singlet sector of a given spin-1/2 Heisenberg model. The NNVB states are in most cases linearly independent [34,35], but the dimension of the subspace they span is much smaller than the singlet sector. Provided the low-energy states of the Heisenberg model are not orthogonal to these states (and there are no reasons for them to be), it should nevertheless be possible in principle to write down an effective Hamiltonian in this basis that reproduces the low-energy spectrum. This Hamiltonian will however in general be very complicated, with matrix elements between all states. Such a description is only useful if the resulting Hamiltonian approximately takes the form of the sum of simple local processes, as postulated by Rokhsar and Kivelson [36], or in other words if the tunneling amplitude between dimer loops is more or less independent of the environment. So any attempt at deriving an effective QDM should address two questions: (i) Can the effective model be approximated by a sum of local processes? (ii) If yes, what is the value of the most important tunneling amplitudes?

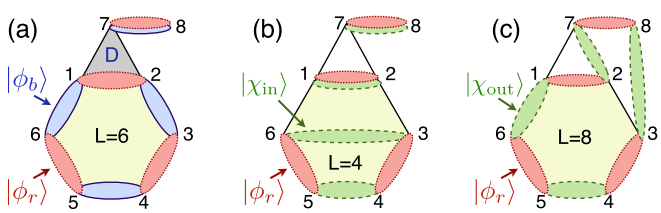

FIG. 1. (Color online) (a) Two NNVB states on the kagome, $|\phi_b\rangle$ and $|\phi_r\rangle$, that are everywhere the same except around a hexagon (ovals denote spin singlets). (b)–(c) The VB coverings $|\chi_{in}\rangle$ and $|\chi_{out}\rangle$ (dashed green ovals) contain long-range singlets that can be virtually excited around the defect triangle "D" of $|\phi_b\rangle$.

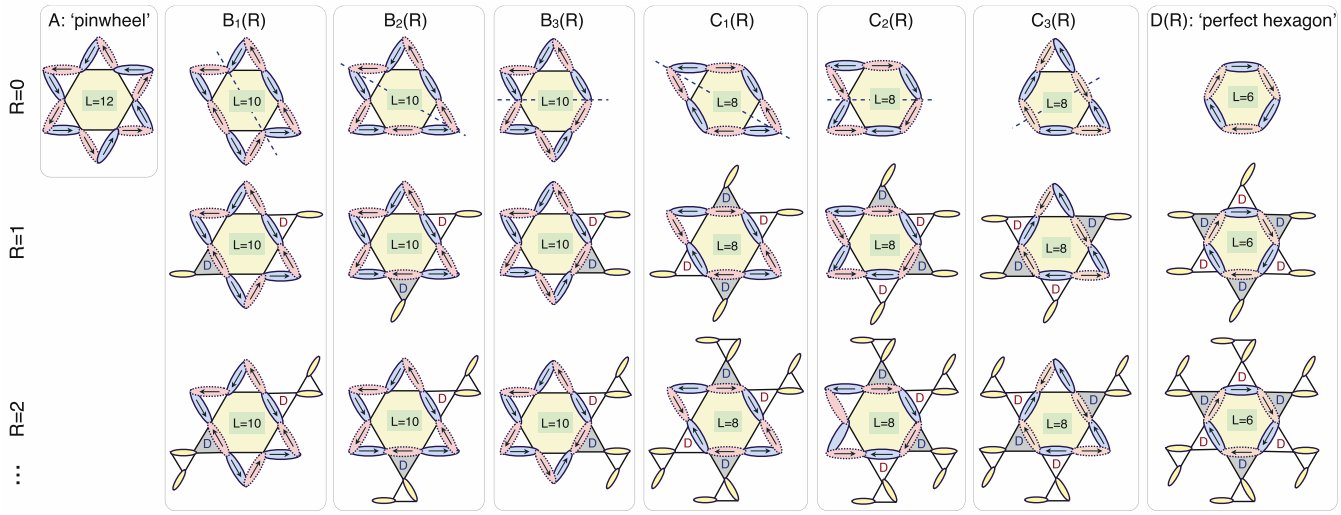

FIG. 2. (Color online) Finite clusters used to extract the dominant tunneling parameters $t_{\rm ED}$ on the kagome. Ovals denote singlets and arrows indicate our singlet orientation [37] convention (clockwise in all hexagons [7]); dashed (blue) lines are reflection symmetries. L denotes the length of the loop formed by the transition graph of the two NNVB states involved in the tunneling process.

The standard approach, pioneered by Rokhsar and Kivelson [7,22,30,36], amounts to truncating the Hamiltonian matrix in the NNVB basis and orthogonalizing the basis, leading to the effective quantum dimer Hamiltonian $\mathcal{H}_{\rm NNVB} = (\mathcal{O}^{-\frac{1}{2}}\mathcal{H}\mathcal{O}^{-\frac{1}{2}})_{\rm NNVB}$, where $\mathcal{O}$ is the overlap matrix. Assuming that the effective Hamiltonian can be written as a sum of local processes that consist of tunneling between two dimer coverings $|\phi_b\rangle$ and $|\phi_r\rangle$ (see first row of Fig. 2 for a sketch of the most important processes), the QDM parameters can in fact be simply determined from the overlap $\langle\phi_b|\phi_r\rangle \equiv \omega$ and the matrix elements $\langle\phi_b|\mathcal{H}|\phi_b\rangle = \langle\phi_r|\mathcal{H}|\phi_r\rangle \equiv E_0$ and $\langle\phi_b|\mathcal{H}|\phi_r\rangle \equiv v$, which can be found from the transition graph following standard rules [7,22,30,32,36,38]. Indeed, the simplicity of the problem allows for a direct evaluation of ${\mathcal{O}_{\rm NNVB}}^{-\frac{1}{2}}$, giving

$$\mathcal{H}_{\rm NNVB} = \begin{pmatrix} E_0 + V_{\rm NNVB} & t_{\rm NNVB} \\ t_{\rm NNVB} & E_0 + V_{\rm NNVB} \end{pmatrix}, \qquad (2)$$

with

$$t_{\rm NNVB} = \frac{v - E_0\omega}{1-\omega^2} \quad \text{and} \quad V_{\rm NNVB} = -t_{\rm NNVB}\omega. \qquad (3)$$

These expressions are identical to Eq. (40) of [22], up to different conventions for the dimer orientation and for the Hamiltonian [39]. This means that for elementary processes the infinite linked-cluster expansion of [22] is equivalent to truncating to the 2×2 NNVB basis of the corresponding finite cluster.

In this approach, the values of $t_{\rm NNVB}$ and $V_{\rm NNVB}$ do not depend at all on the embedding: Indeed, for a given process, clusters corresponding to different rows of Fig. 2 have different E_0 and v, but the same ω and $v - E_0\omega$. So, formulated in this way, the truncation approach leads to the intriguing conclusion that there is no embedding dependence whatsoever.

If this conclusion were correct, it would mean that the low-energy singlet sector of the Hamiltonian on clusters with different embeddings should be identical up to an overall constant. To challenge this conclusion, a natural thing to do is to enlarge the truncation basis to include the *intermediate* longer-range singlets that are generated by applying the Hamiltonian, like $|\chi_{\rm in}\rangle$ for a single hexagon, or $|\chi_{\rm in}\rangle$ and $|\chi_{\rm out}\rangle$ for the 8-site cluster of Fig. 1. Such a basis, denoted by "NNVB+", leads to an effective Hamiltonian $\mathcal{H}_{\rm NNVB+} = (\mathcal{O}^{-1/2}\mathcal{H}\mathcal{O}^{-1/2})_{\rm NNVB+}$ that includes the renormalization from the intermediate long-range singlets and thus the dependence on the environment. It turns out that the low-energy sectors of $\mathcal{H}_{\rm NNVB,+}$ for these two clusters are indeed different from each other as well as from that of the fully truncated Hamiltonian $\mathcal{H}_{\rm NNVB}$ [39]. In particular, the splitting between the low-lying singlets evolves from 1.2 for $\mathcal{H}_{\rm NNVB}$, to $\frac{\sqrt{13}-1}{2} = 1.30277$ for $\mathcal{H}_{\rm NNVB,+}$ of the single hexagon, and finally to 1.15697 for $\mathcal{H}_{\rm NNVB,+}$ of the cluster of Fig. 1. The corresponding reduction for the minimal embedding of the hexagon in the kagome (second row and last column of Fig. 2) is even larger, on account of the many more intermediate states $|\chi_{\rm out}\rangle$ involved (see below). This example shows that there has to be a significant embedding dependence of the tunneling amplitude since it controls the splitting. The rest of this Rapid Communication is devoted to a systematic investigation of this dependence.

To this end, we imagine embedding the minimal clusters shown in the first row of Fig. 2 back on the kagome in such a way that the resulting clusters can only accommodate the two dimer coverings involved in each process. In choosing the clusters that allow us to capture the most important contributions, the spinon picture of the VB dynamics of [40] offers a clear insight. According to this picture, a defect triangle is a bound state of two antikink spinons, and the virtual VB dynamics is due to the motion of such spinons. Following [40], antikinks can only escape our clusters through the dangling (yellow) bonds of the second row of Fig. 2. So to capture the most important fluctuations and to simulate the kagome as close as possible, we proceed by attaching open sawtooth chains of length R next to the defect triangles of the minimal "$R = 0$" clusters. The influence of the remaining environment (most notably, the possible presence of extra defect triangles in the immediate vicinity of the central hexagon) will also be discussed below.

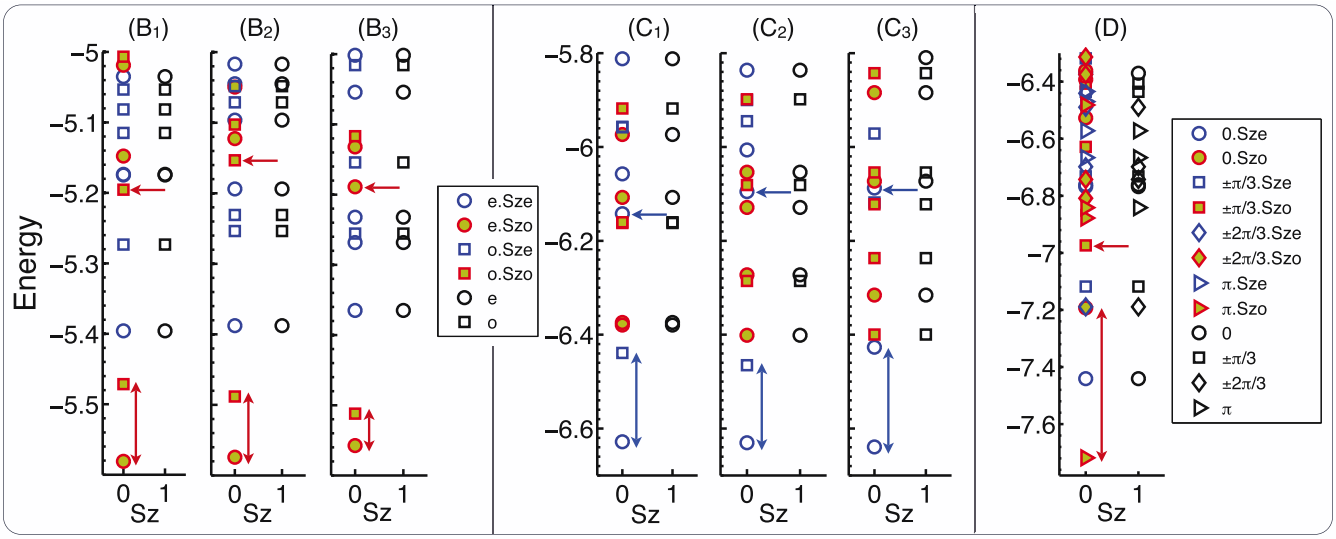

FIG. 3. (Color online) Low-energy spectra of the "$R = 1$" clusters B_1–D of Fig. 2 in the magnetization sectors $S_z = 0$ and 1. Legends: parity under reflection (for B_1–C_3), where "e" and "o" denote even and odd parity, respectively, or angular momenta under sixfold rotations (for D). Spin-inversion parity (for $S_z = 0$) is labeled by "Sze" and "Szo". The two NNVB low-lying singlets are designated by double vertical arrows and the third singlet by horizontal arrows.

When we enlarge the embedding along these lines, the number of intermediate longer-range singlets that need to be included in the truncation basis increases very quickly, rendering the analytical calculation of the matrix elements of $\mathcal{H}_{\mathrm{NNVB}+}$ practically intractable. However, a completely equivalent but technically much simpler method is to use numerical ED in the full singlet basis and extract the effective QDM parameters from the lowest two singlets in the spectrum. The basic idea is that, when the virtual potential energy corrections V_r and V_b of $|\phi_r\rangle$ and $|\phi_b\rangle$, respectively, are the same, then the tunneling amplitude is half the splitting. Now, except for the cluster C_3, in which the reflection operation maps $|\phi_b\rangle \mapsto |\phi_b\rangle$ and $|\phi_r\rangle \mapsto |\phi_r\rangle$, in all remaining clusters the reflection (B_1–C_2) or the sixfold rotation (A, D) map $|\phi_b\rangle \mapsto \eta|\phi_r\rangle$, where $\eta = \pm 1$. This means that $V_r = V_b$ and, moreover, the two eigenstates of the effective QDM, $|\pm\rangle = \frac{|\phi_b\rangle \pm |\phi_r\rangle}{2\sqrt{1\pm\omega}}$, have well-defined parity $\pm\eta$. So we can extract the tunneling amplitude t, including its sign, by simply taking

$$t_{\mathrm{ED}} = \frac{E_+ - E_-}{2}, \tag{4}$$

where E_+ and E_- are the energies corresponding to $|\pm\rangle$, which in turn can be identified in the spectrum by their parity.

For cluster C_3, $|\phi_r\rangle$ and $|\phi_b\rangle$ are not related by any symmetry and thus $V_r \neq V_b$ [41], and $\frac{E_+ - E_-}{2} = [(\frac{V_r - V_b}{2})^2 + t_{\mathrm{ED}}^2]^{1/2}$. Thus we need an independent calculation for $V_r - V_b$ in order to extract t_{ED}. As we show in [39], $|V_r - V_b| \approx 0.005$, which is much smaller than the splitting $|E_+ - E_-|$ found for C_3. So to a very good approximation, $|t_{\mathrm{ED}}| \approx \frac{|E_+ - E_-|}{2}$. The sign of t_{ED} is assumed the same with that of t_{NNVB}, as happens for the other processes.

Some examples of spectra are shown in Fig. 3 for the "$R = 1$" clusters, the values of the tunneling amplitudes deduced in that way are summarized in Table I, and their evolution with the "size" of the embedding is plotted in Fig. 4. These data, which are the main results of this Rapid Communication, contain a lot of important information.

First of all, the singlet sector of the exact spectra shown in Fig. 3 is consistent with the NNVB picture, as we can clearly identify two low-lying singlets (double vertical arrows) with the expected symmetry, that are separated from the third singlet

TABLE I. Tunneling amplitude t_{ED} for the most local processes on the kagome, as extracted from exact diagonalization spectra of the clusters shown in Fig. 2. For comparison, we also give the amplitudes from the NNVB projection (second column).

Process	NNVB	$R = 0$	$R = 1$	$R = 2$	$R = 3$	$R = 4$	$R = 5$
A	0	0	0	0	0	0	0
B_1	$\frac{4}{85} = 0.04705$	+0.09230	+0.05476	+0.04779	+0.04511	+0.04334	+0.04197
B_2	$\frac{4}{85} = 0.04705$	+0.06216	+0.04301	+0.03957	+0.03812	+0.03701	+0.03608
B_3	$\frac{4}{85} = 0.04705$	+0.01952	+0.02272	+0.02496	+0.02562	+0.02564	+0.02544
C_1	$-\frac{4}{21} = -0.19047$	−0.11726	−0.09461	−0.08246	−0.07028		
C_2	$-\frac{4}{21} = -0.19047$	−0.11586	−0.08252	−0.06735	−0.05737		
C_3	$-\frac{4}{21} = -0.19047$	−0.19152	−0.10634	−0.08410	−0.07113		
D	$\frac{3}{5} = 0.6$	$\frac{\sqrt{13}-1}{4} = 0.65138$	+0.26285	+0.14664			

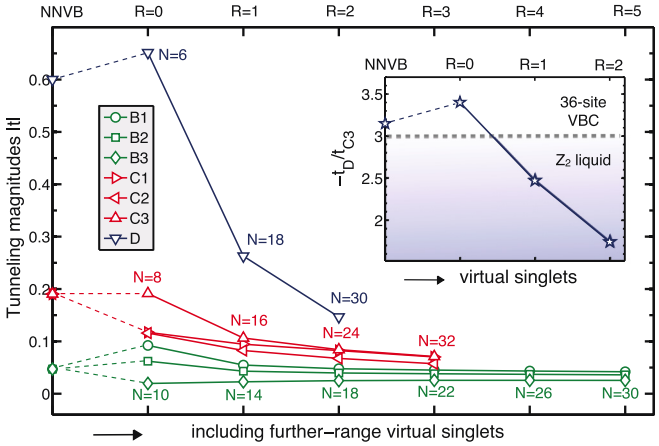

FIG. 4. (Color online) (a) Evolution of $|t|$ as we include further-range virtual singlet fluctuations, quantified by the length R of the sawtooth chains attached to the minimal clusters of the first row of Fig. 2. The NNVB parameters are placed at the origin for comparison. Inset: The ratio of the two strongest processes. The horizontal dashed (gray) line separates the 36-site VBC from the Z_2 spin liquid phase [33].

(horizontal arrow) by an appreciable energy gap [42]. Second, the tunneling amplitude *does* depend on the environment, as expected. The NNVB truncation approach is in reasonable agreement only with the "$R = 0$" clusters C_3 and D, and so it can be considered as an approximate way to calculate the tunneling amplitudes t_{C_3} and t_D without any embedding. However, to describe the kagome antiferromagnet, embedding should be taken into account, and it clearly matters, as demonstrated by the evolution of the parameters with R.

Third, unlike $t_{B_{1-3}}$ and $t_{C_{1-3}}$, which converge quickly with R, the amplitude $t_D(R)$ for the "perfect hexagon" process shows a remarkable drop from 0.65138 at $R = 0$ to 0.26285 at $R = 1$, and a similarly high drop to 0.14664 at $R = 2$. This shows that fluctuations have the strongest influence on the process with the largest number of defect triangles (and spinons [43]). Hence, the 36-site VBC favored by the "perfect hexagon" process D is clearly disfavored by virtual fluctuations (see below). Note that the "$R = 3$" cluster of type (D) has $N = 42$ sites, which is too large for an ED treatment, given the small number of available symmetries. However, the three available ED data suggest a convergence at $R \gtrsim 4$–5, and it is likely that its value will converge slightly below that of $t_{C_{1-3}}$. The reason why convergence is slowest in (D) is related to statistical pressure (spinons are fermions on kagome [40]) which tends to push spinons out of the clusters; the more spinons the higher the pressure, and thus the longer the chains needed to accommodate the escaping spinons.

Fourth, as we show in [39], already for "$R = 2$" clusters, the tunneling amplitude of some processes starts to depend on the remaining environment besides the sawtooth chains. This shows that a description in terms of a QDM with "local" processes can only be approximate. However, most processes still have the same amplitude at the level "$R = 2$," and those which take different values have a small dispersion except for very rare configurations with an anomalously large concentration of defect triangles. So it is still possible to define an approximate description with "average" tunneling amplitudes.

The potential terms of the QDM can be extracted in a similar way with the help of a numerical linked-cluster procedure [39]. The resulting data show that the binding energy of two defect triangles $V_{2-\mathrm{dt}}$ can be essentially neglected, but the binding energy $V_{3-\mathrm{dt}}$ between three defect triangles around a hexagon (process D) is large and positive. The specific values depend again on the embedding (0.18470 for $R = 1$ and 0.09718 for $R = 2$), but they are of the same order of magnitude as the corresponding tunneling, so they must be taken into account. Importantly, the fact that $V_{3-\mathrm{dt}}$ is positive (in contrast to series expansions around the perturbative dimerized limit [18]) means that virtual fluctuations penalize the "perfect hexagons" not only by the strong reduction in t_D but also via the potential terms.

Discussion. In their recent study of the unconstrained QDM model, Poilblanc *et al.* [22,23] interpolated between the Heisenberg point (in its truncated NNVB treatment) and the exactly solvable spin-liquid point of Misguich *et al.* [7], while Läuchli [33] examined the fate of the QDM as a function of the ratio between the two strongest tunneling processes, i.e., t_D and t_C. Both studies showed that the system is extremely close to a quantum critical point, separating the 36-site VBC state from a Z_2 spin liquid phase. While it is possible that the two liquid phases are adiabatically connected to each other, the path in the parameter space taken in [33] is more directly connected to the present findings, since t_D and $t_{C_{1-3}}$ are the strongest and also the ones that are affected the most by virtual fluctuations. According to [33], the GS of the model turns into a Z_2 spin liquid already at $-t_D/t_C \sim 3$, and including the potential terms would probably shift this boundary even higher. In any case, as shown in Fig. 4 (inset), the ratio $-t_D/t_{C_3}$ goes way below this boundary, meaning that we are deep inside the Z_2 spin liquid phase. It would be interesting to check explicitly whether the more precise model that includes the dependence on the remaining environment and the potential terms leads to the same phase, a plausible result since the average model is deep in the Z_2 spin liquid phase. This is left for future investigation.

Acknowledgments. We would like to thank A. M. Läuchli for enlightening discussions and M. Mambrini for fruitful correspondence. This work was partly supported by the Deutsche Forschungsgemeinschaft (DFG) under the Emmy-Noether program, by the Swiss National Fund, and by the US Department of Energy, Office of Basic Energy Sciences, Division of Materials Sciences and Engineering, under Award No. DE-FG02-08ER46544.

[1] P. W. Anderson, Mater. Res. Bull. **8**, 153 (1973).
[2] P. Fazekas and P. W. Anderson, Philos. Mag. **30**, 423 (1974).
[3] P. W. Anderson, Science **235**, 1196 (1987).
[4] S. Liang, B. Doucot, and P. W. Anderson, Phys. Rev. Lett. **61**, 365 (1988).
[5] A. P. Ramirez, Annu. Rev. Mater. Sci. **24**, 453 (1994).

[6] S. Sachdev, Phys. Rev. B **45**, 12377 (1992).
[7] G. Misguich, D. Serban, and V. Pasquier, Phys. Rev. Lett. **89**, 137202 (2002).
[8] G. Misguich, D. Serban, and V. Pasquier, Phys. Rev. B **67**, 214413 (2003).
[9] L. Balents, Nature (London) **464**, 199 (2010).
[10] M. Shores, E. Nytko, B. Barlett, and D. Nocera, J. Am. Chem. Soc. **127**, 13462 (2005).
[11] T.-H. Han, J. S. Helton, S. Chu, D. G. Nocera, J. A. Rodriguez-Rivera, C. Broholm, and Y. S. Lee, Nature (London) **492**, 406 (2012).
[12] Y. Ran, M. Hermele, P. A. Lee, and X. G. Wen, Phys. Rev. Lett. **98**, 117205 (2007).
[13] M. Hermele, Y. Ran, P. A. Lee, and X. G. Wen, Phys. Rev. B **77**, 224413 (2008).
[14] O. Ma and J. B. Marston, Phys. Rev. Lett. **101**, 027204 (2008).
[15] Y. Iqbal, F. Becca, S. Sorella, and D. Poilblanc, Phys. Rev. B **87**, 060405 (2013).
[16] J. B. Marston and C. Zeng, J. Appl. Phys. **69**, 5962 (1991).
[17] P. Nikolic and T. Senthil, Phys. Rev. B **68**, 214415 (2003).
[18] R. R. P. Singh and D. A. Huse, Phys. Rev. B **76**, 180407(R) (2007).
[19] A. V. Syromyatnikov and S. V. Maleyev, Phys. Rev. B **66**, 132408 (2002).
[20] R. Budnik and A. Auerbach, Phys. Rev. Lett. **93**, 187205 (2004).
[21] G. Evenbly and G. Vidal, Phys. Rev. Lett. **104**, 187203 (2010).
[22] D. Schwandt, M. Mambrini, and D. Poilblanc, Phys. Rev. B **81**, 214413 (2010).
[23] D. Poilblanc, M. Mambrini, and D. Schwandt, Phys. Rev. B **81**, 180402(R) (2010).
[24] D. Poilblanc and G. Misguich, Phys. Rev. B **84**, 214401 (2011).
[25] L. Messio, B. Bernu, and C. Lhuillier, Phys. Rev. Lett. **108**, 207204 (2012).
[26] S. Capponi, V. R. Chandra, A. Auerbach, and M. Weinstein, Phys. Rev. B **87**, 161118 (2013).
[27] S. Yan, D. A. Huse, and S. R. White, Science **332**, 1173 (2011).
[28] S. Depenbrock, I. P. McCulloch, and U. Schollwöck, Phys. Rev. Lett. **109**, 067201 (2012).
[29] A. W. Sandvik, Phys. Rev. Lett. **95**, 207203 (2005).
[30] C. Zeng and V. Elser, Phys. Rev. B **51**, 8318 (1995).
[31] V. Elser, Phys. Rev. Lett. **62**, 2405 (1989).
[32] M. Mambrini and F. Mila, Eur. Phys. J. B **17**, 651 (2000).
[33] A. M. Läuchli, talk at KITP, October 31, 2012, http://online.kitp.ucsb.edu/online/fragnets12/laeuchli.
[34] A. Seidel, Phys. Rev. B **80**, 165131 (2009).
[35] J. Wildeboer and A. Seidel, Phys. Rev. B **83**, 184430 (2011).
[36] D. S. Rokhsar and S. A. Kivelson, Phys. Rev. Lett. **61**, 2376 (1988).
[37] An arrow on bond ij oriented from i to j corresponds to the spin singlet state $(\uparrow_i\downarrow_j - \downarrow_i\uparrow_j)/\sqrt{2}$.
[38] B. Sutherland, Phys. Rev. B **37**, 3786 (1988).
[39] See Supplemental Material at http://link.aps.org/supplemental/10.1103/PhysRevB.90.100406 for (i) the basic elements of the fully truncated NNVB method, (ii) the analytical treatment of the perfect hexagon process, (iii) the influence of extra defect triangles in the vicinity of the tunneling loop, and (iv) the treatment of the potential terms.
[40] Z. Hao and O. Tchernyshyov, Phys. Rev. B **81**, 214445 (2010).
[41] Physically, this can be understood by noting that the distance between the two defect triangles involved in $|\phi_b\rangle$ is different from that in $|\phi_r\rangle$.
[42] We remark that the presence of low-lying triplets in clusters C_1-C_3 and particularly in D is not incompatible with the NNVB picture, provided that the spin gap remains open in the thermodynamic limit.
[43] Given that dimers move by passing spinons (see discussion above), the effect of virtual fluctuations intensifies with the number of spinons involved (zero, two, four, and six in clusters A, B, C, and D, respectively).